

A comparative study of the spatial averaging in ∇ and \times -probes for the measurements of streamwise and spanwise velocities in wall turbulence

J. Philip, R. Baidya, N. Hutchins, J. P. Monty and I. Marusic

Department of Mechanical Engineering
 The University of Melbourne, Victoria, 3010 AUSTRALIA

Abstract

Spatial resolution of cross-wires placed in a turbulent boundary layer is investigated using the DNS channel-flow database of del Álamo *et al.* [2]. Specifically, various configurations of ∇ and \times -probes are considered and the effects of varying wire length, l^+ and the spacing between the center of the two wires, Δs^+ , on the measured stream and spanwise velocities, u and v respectively, are studied (for a fixed inclination angle of the wires to the stream-wise direction x , $\theta = 45^\circ$). The simulations show that there is an ‘error cancelation’ mechanism present in the \times -probe which when combined with the increased correlation along the wall-normal direction with increasing z , and physical possibility to reduce Δs in \times -probes (compared to ∇ -probes) means that \times -probes are better suited for stream-spanwise velocity measurements than ∇ -probes in wall-turbulence.

Introduction

The averaging issues with single hot-wires have resurfaced in recent years with new investigations into the scaling of the ‘inner peak’ in the streamwise velocity variance. It is well documented by Hutchins *et al.* [5] and Ng *et al.* [7] that there is a significant attenuation in the streamwise velocity variance with increasing wire length. Over the past years relatively high Reynolds number Direct Numerical Solution (DNS) databases are becoming available and have been employed to study the effect of wire-length on the attenuation of the second order statistics for standard hot-wires (with one wire), e.g. [1]. However, very few investigations have been devoted to two-wire probes. There are two notable exceptions. First is that of Moin and Spalart [6], which marks the first study of this kind at Re_τ ($= u_\tau \delta / \nu$, where δ is the turbulent boundary layer thickness, u_τ , the friction velocity and ν , the kinematic viscosity) of 180. Second is the more detailed investigation undertaken by Suzuki and Kasagi [8] at $Re_\tau = 150$ for both single and cross-wires, however, concentrating primarily on the effect of wire separation rather than spatial averaging in cross-wires. A need for a higher Re_τ investigation is motivated by the discovery of large scale motions in the log region of the turbulent boundary layer (TBL), which affect the small scales close to the wall [4].

Here we evaluate the effects of the finite dimension of ∇ and \times -probes using the DNS simulation database of del Álamo *et al.* [2] at $Re_\tau=934$.

Methodology

The schematics of ∇ and \times -probe are shown in figures 1(a) and (b), respectively. There are three parameters which can be used to categorize ∇ and \times -probes, namely, the inclination angle of the wires with respect to the streamwise velocity, θ (0° when wire is aligned with the streamwise direction and 90° for spanwise alignment), the length of the wires (assuming both the wires are of the same length), l^+ , and the spacing between the wire-midpoints, Δs_y^+ (for ∇ -probes), or Δs_z^+ (for \times -probes). Note that the superscript, $+$ denotes normalization with wall units. Here, x , y and z are the streamwise, spanwise and wall-

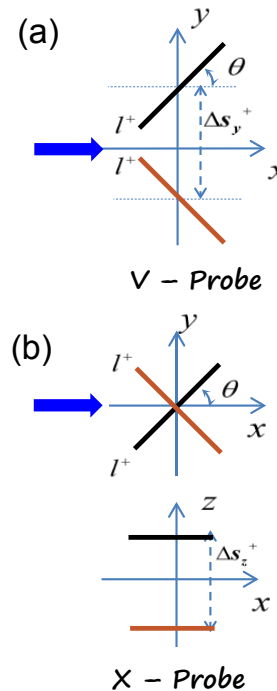


Figure 1: Schematic of the ∇ and \times -probe.

normal directions (with u , v and w , the corresponding velocity components).

Both ∇ and \times -probes are simulated using the DNS database of del Álamo *et al.* [2] which has a spatial discretization of Fourier \times Fourier \times Chebyshev with grid points $N_x \times N_y \times N_z = 3072 \times 2304 \times 385$ in streamwise, spanwise and wall-normal directions. The computational domain is $8\pi h$ units in the streamwise direction and $3\pi h$ units in the spanwise direction, where h is the half channel height. After de-aliasing in the Fourier domain, the equivalent resolution in real domain for streamwise and spanwise directions is $\Delta x^+ \times \Delta y^+ \approx 11.46 \times 5.73$ in wall units. However, due to the $3/2$ de-aliasing rule, in real domain the available database has velocity field on an interpolated grid with a of resolution 7.6×3.8 . And this is the resolution that is presented in the figures below, to be consistent with previous studies (e.g., [1]). In the wall-normal direction, the grid spacing increases from $\Delta z^+ \approx 0.03$ at the wall to a maximum 7.6 at the center of the channel.

Simulation of the ∇ and \times -probes follows the usual assumptions employed for single wires, such as, (i) very large l/d , (where, d is the diameter of the wire). (ii) No effect of the temporal response of the hot-wire is considered, i.e, a flat frequency response is assumed. (iii) For each wire, locally the velocity on the homogeneous plane is decomposed into normal and paral-

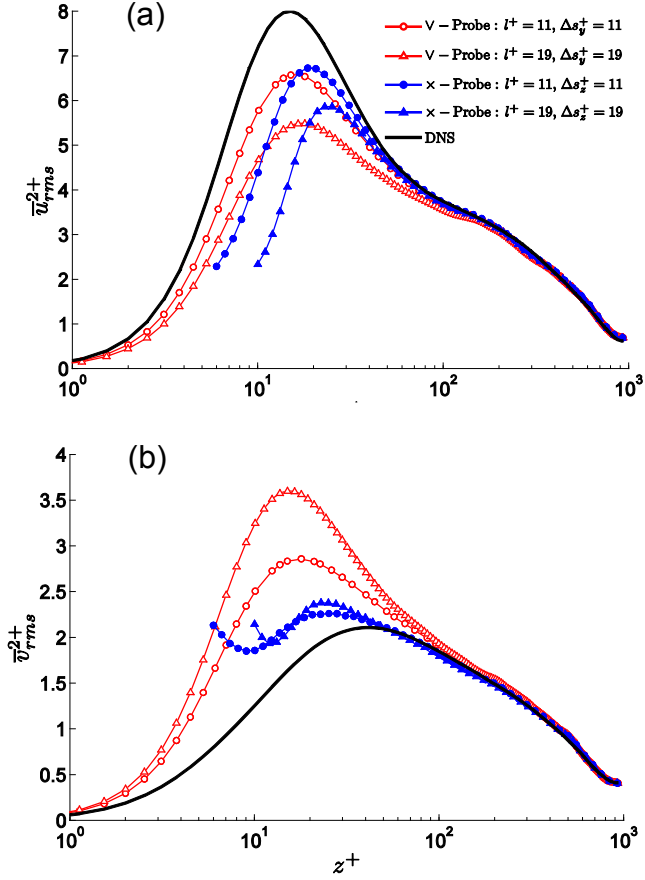


Figure 2: Variation of variances with z -locations for ∇ and \times -probe at $\theta = 45^\circ$. The full (black) line is the un-averaged DNS results, whereas open and closed symbols correspond to ∇ and \times -probes, respectively. (a) u_{rms}^2+ . (b) v_{rms}^2+ .

lel components w.r.t the wire. The effective cooling velocity for each wire is calculated using only the normal component. There is a small and non-significant effect of the parallel component of the velocity that has been observed; however, this is not presented here to focus on the wire separation and averaging effects. (iv) A linear box-filter is used to calculate the effective velocity for each wire. We have observed (though not included here) that linear-filtering is sufficient and compares favourably to actual experiments at matched l^+ and Re_τ . (v) Once effective velocities corresponding to wire 1 and 2 are calculated, following the usual procedure of cross-wire calculations, two linear equations are obtained which are inverted to obtain the ‘measured’ u and v , denoted here by \bar{u} and \bar{v} (e.g., [6]).

Results

As mentioned above, there are three parameters that govern the resolution issues in ∇ and \times -probes, namely, θ , l^+ and Δs_y^+ (for ∇ -probes), or Δs_z^+ (for \times -probes). However, here we concentrate only on the case where $\theta = 45^\circ$. The two main reasons are: (i) $\theta = 45^\circ$ is the most commonly used configuration in the experiments. (ii) Several different simulations with varying θ have been performed (not shown here), and the results indicate that increasing θ from 0° to 45° causes the attenuation to increase rapidly, which does not change much with further increase in θ . And this can be explained from the two-point correlation of velocity over the wire length wherein the correlation drops rapidly from 0° to 45° and thereafter remaining relatively unchanged.

Figures 2(a) and (b) illustrate the effects of l^+ and Δs^+ on the streamwise and spanwise variances for two typical configurations of ∇ and \times -probes at $\theta = 45^\circ$. The thick (black) lines are the DNS results without any averaging; the empty (red) and filled (blue) symbols are for the ∇ and \times -probes, respectively. Two cases considered are: $l^+ = \Delta s_y^+ = 11$ and 19 (for ∇ -probe), and $l^+ = \Delta s_z^+ = 11$ and 19 (for \times -probe). It can be observed that in general the u_{rms}^2+ are under-predicted whereas the v_{rms}^2+ are over-predicted by the probes. The reason for this is evident from examining the cross-wire equations that are employed to recover the velocities:

$$\bar{u} = \frac{\tilde{u}_1 + \tilde{u}_2}{2} + \frac{\tilde{v}_1 - \tilde{v}_2}{2}; \quad \bar{v} = \frac{\tilde{u}_1 - \tilde{u}_2}{2} + \frac{\tilde{v}_1 + \tilde{v}_2}{2}, \quad (1)$$

where, \bar{u} is the ‘measured’ u -velocity, \tilde{u}_1 and \tilde{u}_2 are the velocities averaged over wires 1 and 2, assigned to the midpoints of the wires. And similar definitions hold for the v -velocities too. Notice that \tilde{v}_1 and \tilde{v}_2 are much smaller in magnitude compared to \tilde{u}_1 and \tilde{u}_2 ; so, neglecting them (as a first approximation), \bar{u} is simply the average of \tilde{u}_1 and \tilde{u}_2 , whereas, \bar{v} is their difference. Therefore the variance of \bar{u} , $\overline{u_{rms}^2+}$ in figure 2(a) is lower than the DNS distribution, and since the difference of two large numbers will return a large variance, $\overline{v_{rms}^2+}$ is higher than the corresponding DNS distribution in figure 2(b).

A closer look at figures 2(a) and (b) shows that there are more subtle effects that are noticeable. For instance, in figure 2(a) at $z^+ = 15$ (the approximate peak of u_{rms}^2+ , for the same l^+ and Δs^+ , the ∇ -probe seems to exhibit a lesser error than the \times -probe, whereas moving to a higher z^+ shows that errors in the \times -probe have reduced compared to the ∇ . Furthermore, in figure 2(b), say at $z^+ = 15$, ∇ -probes have higher errors than the \times counterparts and this error does not seem to be affected by changing the z -locations. Apart from the general differences between ∇ and \times -probes, there are also differences among different geometrical configurations of ∇ and \times -probes themselves. For example, two ∇ -probes with different l^+ and Δs_y^+ will also be different, and same holds for \times -probe. Some of these observations may be intuitive but most are not. To probe further into these errors, it is best to consider a single z -location and analyze the ∇ and \times -probe separately in detail, with varying Δs^+ and l^+ .

The effects of l and Δs on u_{rms} and v_{rms} are studied in detail in figure 3 for the ∇ and \times -probes at $z^+ = 15$ and $\theta = 45^\circ$. Figures 3(a,b) and (c,d) show, respectively for ∇ and \times -probes an error, or a relative difference ($\mathcal{R}\mathcal{D}$) from the actual DNS data i.e., $(\bar{u}^2+ - \bar{u}_{DNS}^2+)/\bar{u}_{DNS}^2+ =: \mathcal{R}\mathcal{D}_u$ for streamwise velocity, and a similar definition for spanwise velocity.

As mentioned previously, in general, $\mathcal{R}\mathcal{D}_u$ is negative whereas $\mathcal{R}\mathcal{D}_v$ is positive. Even though this is strictly true for $\mathcal{R}\mathcal{D}_u$, the same does not hold for $\mathcal{R}\mathcal{D}_v$. Figure 3(d) shows that even though for smaller wire-lengths $\mathcal{R}\mathcal{D}_v$ is positive, with increasing l^+ it does become negative. We shall return to this point further below.

It is pointed out that if two points are well correlated in space the averaging issues are less between them, whereas the averaging issues are most significant where there are regions of low correlation. If there is a (hypothetical) region over which the correlation is unity, spatial averaging does not affect the measurements. This shows that a significant understanding of the spatial averaging in sensors can be obtained by the knowledge of the 3-D correlation maps over the sensor. In our specific case, we are interested in correlations along the wire length or at most over a plane. We do not present the maps of correlations here for the sake of brevity, however, the significant results will be summarized as an aid to understand the various effect of l^+ and

Δs^+ on ∇ and \times -probes.

For ∇ and \times -probes, in the case of both u_{rms} and v_{rms} , increasing l^+ is always accompanied by a decrease in $\mathcal{R}\mathcal{D}$ - this is the effect of spatial averaging along the wire, and there are no exceptions. The spatial averaging always reduced the variance (because in a turbulent flow the correlations always reduce), a well known fact from the studies on single hot-wires. Depending upon the direction of the wire, the averaging can be less or more. For example, if the wire is at 90° (i.e., along spanwise direction), there is large averaging due to the rapid decay of the correlations along that direction (linked to the wall streaks, if the probe is near the wall), whereas much less along the streamwise direction. Knowledge of the correlations can be used to predict almost exactly the spatial averaging along the wires using an expression similar to that which was first derived by [3].

For the same Δs^+ , say ≈ 19 , figures 3(a) and (c) show that the error in u -variance for the ∇ -probe is less than that of the \times -probe; the reason being a faster drop of u -correlation along the wall-normal direction compared to the spanwise direction at $z^+ = 15$.

The values of $\mathcal{R}\mathcal{D}_v$ are mostly positive for the ∇ -probe because, as mentioned above, while extracting the velocities out from the two wires the \bar{v} (the measured v) is the difference of u from the two wires. This combined with the decreasing effect of l^+ on $\mathcal{R}\mathcal{D}_v$ results in the distribution shown in figure 3(b). This competing effects can even make the error vanish, which of course does not mean that there are no finite dimension errors. This is physically understandable because measurements with longer wires, with the same Δs will be better correlated with each other, than a shorter one - producing a counter-intuitive result of longer wires performing better than the short ones.

In the case of \times -probe for $\mathcal{R}\mathcal{D}_v$, yet another effect comes into play - the averaging effect of v (corresponding to the second term in equation (1) for \bar{v} which was ignored as being small in the above case, however, is not so small here), which tends to decrease $\mathcal{R}\mathcal{D}_v$. Thus, for \times -probe there are two effects which decrease $\mathcal{R}\mathcal{D}_v$, and one that increases, and this makes the reduction of $\mathcal{R}\mathcal{D}_v$ (or reduction in errors) an efficient process in \times -probes compared to the ∇ -probes. This in turn makes \times -probes a 'more accurate' one for spanwise velocity measurements than ∇ -probes.

From a practical point of view for a ∇ -probe not all Δs_y are feasible. For instance, in the case of $\theta=45^\circ$, Δs_y can not be smaller than $l/\sqrt{2}$, else the two wires will try to occupy the same physical space. This constraint is represented in figures 3(a,b) with a thick (grey) dashed line. The analogous constraint for \times -probe is the positivity of Δs_z , which is shown similarly in figures 3(c,d). The shaded areas in the figures are 'inaccessible regions' due to physical constants. Practically, it suggests that for a given wire length the best option (i.e., least errors) are attained by remaining as close as possible to the grey dashed lines. It is clear that there is much more flexibility with an \times -probe to reduce errors. Increasing z makes the \times -probe better even for u_{rms} (c.f. figure 2(a)) due to the increased u -correlation in z -direction for higher z .

As a word of caution, it should be mentioned that the above analysis pertains to second order statistics, and in fact, a probe could be built in such a way (c.f. figure 3) that the variance errors could be made negligible. However, this does not mean that the measurements are 'correct'; the higher order statistics and the instantaneous velocity signal would still be corrupted by spatial averaging and wire-separation effects. The analysis serves the purpose of understanding the origin of the errors in the variances - which is by-far the most commonly accepted

measure of errors in hot-wires.

Summary and conclusions

The ∇ and \times -probes for the measurements of streamwise and spanwise velocities are studied using a DNS database at $Re_\tau = 934$ to understand the effect of finite dimensionality of the sensors on the measured variances.

There are three parameters that are used to categorize ∇ and \times -probes, namely, the inclination angle of the wires with respect to the streamwise velocity, θ , the length of the wires, l , and, the spacing between the wires, Δs_y (for ∇ -probes), or Δs_z (for \times -probes). The present work is restricted to $\theta = 45^\circ$. The results show that the measurements with ∇ and \times -probes, in general, results in a negative error for u_{rms} and a positive one for v_{rms} . The effect of l is to always attenuate the measurements (i.e., to make the errors negative). This, sometimes, opposing effects of l and Δs_z in \times -probes can even make the errors in v_{rms} vanish for practically feasible probes.

Finally, because of the 'error cancelation' effects present in the \times -probe, the increased correlation along the wall-normal direction with increasing z , and physical possibility to reduce Δs_z , it could be said that \times -probes are better suited for uv (stream-spanwise velocity) measurements than ∇ -probes in wall-bounded turbulent flows.

Acknowledgements

The authors gratefully acknowledge support from the Australian Research Council.

References

- [1] Chin, C. C., Hutchins, N., Ooi, A. S. H. and Marusic, I., Use of direct numerical simulation (DNS) data to investigate spatial resolution issues in measurements of wall-bounded turbulence, *Meas. Sci. Technol.*, **20**, 2009, 115401.
- [2] del Álamo, J. C., Jiménez, J., Zandonade, P. and Moser, R. D., Scaling of the energy spectra of turbulent channels, *J. Fluid. Mech.*, **490**, 2003, 37–74.
- [3] Dryden, H. L., Schubauer, G. B., C. Mock, J. and Skramstad, H. K., Measurements of intensity and scale of wind tunnel turbulence and their relation to the critical Reynolds number of spheres, Technical report, NACA Report 581, 1937.
- [4] Hutchins, N. and Marusic, I., Large-scale influences in near-wall turbulence, *Phil. Trans. R. Soc. A*, **365**, 2007, 647–664.
- [5] Hutchins, N., Nickels, T. B., Marusic, I. and Chong, M. S., Hot-wire spatial resolution issues in wall-bounded turbulence, *J. Fluid. Mech.*, **635**, 2009, 103–136.
- [6] Moin, P. and Spalart, P. R., Contributions of numerical simulation data bases to the physics, modeling, and measurement of turbulence, Technical report, NASA Tech. Memo 100022, 1987.
- [7] Ng, H. C. H., Monty, J. P., Hutchins, N., Chong, M. S. and Marusic, I., Comparison of turbulent channel and pipe flows with varying Reynolds number, *Exp. Fluids*, **51**, 2011, 1261–1281.
- [8] Suzuki, Y. and Kasagi, N., Evaluation of hot-wire measurements in wall shear turbulence using a direct numerical simulation database, *Exp. Therm. Fluid Sci.*, **5**, 1992, 69–77.

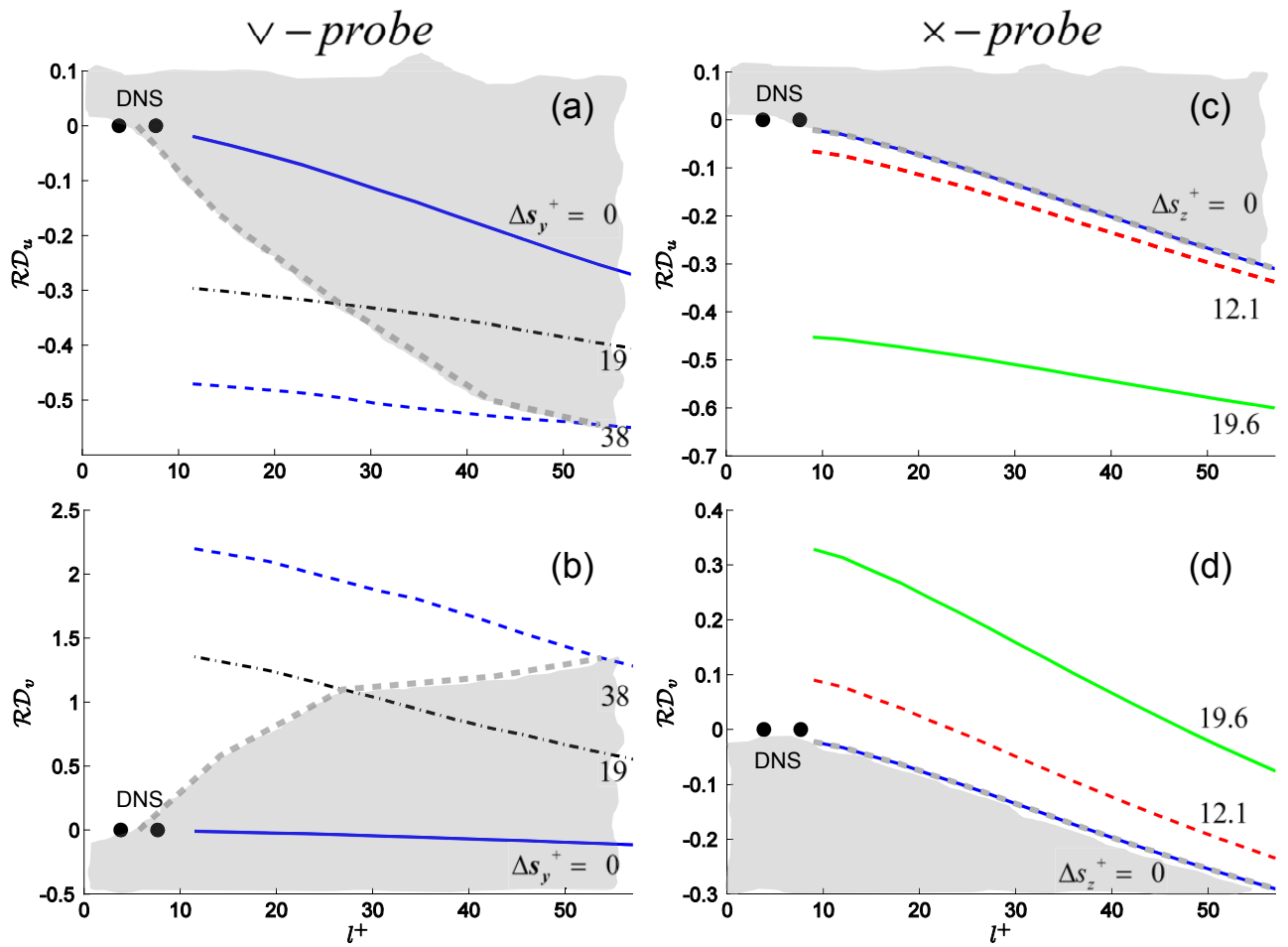


Figure 3: Distributions of the relative difference (\mathcal{RD}) for various configurations of \vee and \times -probes at $\theta = 45^\circ$ from the un-averaged DNS data. (a) \mathcal{RD}_u for \vee -probes. (b) \mathcal{RD}_v for \vee -probes. (c) \mathcal{RD}_u for \times -probes. (d) \mathcal{RD}_v for \times -probes. The grey region separated by thick grey lines show regions which correspond to probes which are physically infeasible to manufacture.